Mesoporous silica sphere-polysulfone mixed matrix membranes for gas separation

*Beatriz Zornoza, Silvia Irusta, Carlos Téllez, Joaquín Coronas**

Department of Chemical and Environmental Engineering, University of Zaragoza, 50018 Zaragoza, Spain. Tel: +34 976 762471. Fax: +34 976 761879.

Nanoscience Institute of Aragon, University of Zaragoza, 50009 Zaragoza, Spain.

*Corresponding author. E-mail: coronas@unizar.es

ABSTRACT. A series of mixed matrix membranes were prepared comprising polysulfone Udel® matrix and ordered mesoporous silica spheres as filler with loadings varying between 0 and 32 wt.%. The interaction between the filler and the polymer was studied by scanning and transmission electron microscopy, thermogravimetry, differential scanning calorimetry and dynamic mechanical analyses, N_2 porosity, X-ray photoelectron spectrometry and attenuated total reflectance-Fourier transform infrared spectroscopy. All these characterizations allowed us to infer an optimum interaction based on both the penetration of the polymer chains into the mesoporosity of the silica spheres and the establishment of hydrogen bondings between the hydroxyl-rich surface and the aryl ether groups of the polymer. An optimum loading of 8 wt.% was found in terms of H_2/CH_4 separation performance. In addition, the optimum membrane was tested for CO_2/N_2 separation.

KEYWORDS. Mixed matrix membrane; Gas permeation; Ordered mesoporous silica spheres; Polysulfone.

INTRODUCTION

Membrane processes have received significant attention as a promising technology for the separation of gaseous mixtures and for gas purification processes. They represent a viable commercial alternative due to their high efficiency, easy intensification, simple operation and low capital and operating costs, among other advantages, compared to traditional separation processes such as adsorption, low-temperature condensation or cryogenic distillation, or combinations of these[1-3]. However, it has been recognized that there is a trade-off between the key parameters for gas separation, permeability and the separation factor, as the latter decreases with increasing permeability of the selectively transported gas component[4]. Over the last decade, in order to establish a membrane with higher gas separation performance relative to the bare polymeric membrane material, various polymers have been modified to produce mixed matrix membranes (MMMs) with the incorporation of inorganic fillers, such as zeolites[5], ordered mesoporous silica[6-8], non-porous silica[9, 10], carbon molecular sieves[11], and carbon nanotubes[12, 13] among others. When using nanoporous materials, MMMs have the advantage of combining the benefits of both phases: the superior gas transport properties and thermal resistance of molecular sieves with the desirable mechanical properties, low price and good processability of polymers[14, 15].

Polysulfone (PSF) is one of the most common amorphous glassy polymers used for gas membrane separation. A considerable research effort has examined the use of nanoporous materials in PSF-based MMMs[5-8, 16]. Glassy polymers, such as polysulfone Udel® which presents a rigid and high-strength structure, frequently offer better transport performance for specific gas permeation mixtures when compared to rubbery materials, but have the disadvantage of poor polymer chain mobility during the membrane formation. This rigid mobility may result in a weak interaction between microporous fillers such as zeolites and the polymer due to its inadequate wetting. If polymer chains are not completely able to surround microporous zeolite, undesirable channels may be created between both phases[1, 6]. This fact induces higher permeabilities because of the by-passing gas effect accompanied by losses of selectivity. Consequently, the challenge is to avoid these undesirable gaps between the filler

and the rigid polymer to achieve high performance of both permeability and selectivity in gas separation. Among other strategies previously used to enhance interaction between inorganic material and polymer, zeolite Beta-polysulfone membranes have been soaked with p-xylenediamine/methanol solution[17], zeolite A surfaces have been modified with the silane coupling agent(3-aminopropyl)-diethoxymethyl silane to produce zeolite A-polyethersulfone MMMs[18], and zeolite Beta nanocrystals have been synthesized by hydrothermal synthesis inside a Nafion membrane[19]. The use of high silica content, hydrophobic zeolites, such as Nu(6)-2, is also an efficient way to improve adhesion with PSF[5].

The application of mesoporous materials rather than microporous fillers may improve the filler-polymer contact and result in a selective film. The size and shape selectivity (typical of microporous materials) would then be combined or replaced by improved interfacial properties (typical of mesoporous materials)[20]. Mesoporous materials have large pores (2-50 nm) and polymer chains may consequently be able to penetrate into the mesopores as cross sectional areas per chain[21] for synthetic polymers are around 1 nm^2 or less. This value has been verified by TEM analysis, and an apparent diameter of 0.9-1.2 nm was measured for a single PSF chain[22]. Furthermore, ordered mesoporous silicas such as MCM-41[23] and MCM-48[24] have wall thicknesses in the 1 nm range and pore diameters of about 2-5 nm. The pore diameter would allow the penetration of the PSF chains into the mesoporosity of the filler, which would help the formation of intimate composites. In fact, in a single particle of ordered mesoporous silica, because of the nanometer thickness of the silica wall, the periodicity would be transferred from the silica to the embedded polymer, as the preparation of ordered mesoporous carbons using ordered mesoporous silica templates (MCM-48) suggests[25].

In addition, ordered mesoporous silicas have large surface areas with hydroxyl groups (2-4 $\mu mol/m^2$)[26] which can be bonded through hydrogen-bonding to the aryl ether oxygen atoms present, for instance, in PSF-type polymers[6]. This together with the high variety of particle shape and size and pore diameter makes these materials (e.g. MCM-41[6, 8] and MCM-48[7]) suitable for the development of a new generation of MMMs. The aim of this study is the preparation and characterization of ordered mesoporous silica sphere-polysulfone mixed matrix membranes (MSS-PSF MMMs) with an optimum

amount of inorganic filler able to produce an enhancement in terms of H_2/CH_4 and CO_2/N_2 separation performance. The working hypothesis is that spherical particles of ordered mesoporous silica MCM-41 with narrow particle size distribution would facilitate the preparation of highly homogeneous MMMs. The main advantage of our research, when compared to previous results using MCM-41[6, 8] or MCM-48[7], is related to the use of MCM-41 in the form of 2-4 μm spheres. This minimizes agglomeration and hence improves dispersability and interaction with the polymer for two reasons: i) the spherical shape limits the contact between silica particles, ii) the 2-4 μm spherical particles provide a lower external surface area to volume ratio than that used in other reports (for instance, with 80 ±30 nm MCM-41 particles[8]).

EXPERIMENTAL SECTION

Synthesis of mesoporous silica spheres (MSSs)

MSSs were prepared as described in the literature[27] but including minor variations in the molar composition of the synthesis sol[28]. To synthesize the MSSs used in this work a source of silica (sodium metasilicate, Na_2SiO_3, Sigma-Aldrich, St. Louis, MO), a surfactant (cetyltrimethylammonium bromide (CTABr), $C_{19}H_{42}NBr$, Sigma-Aldrich, St. Louis, MO), responsible for the mesoporous structure, and finally an initiator for the colloidal aggregates formation (ethylacetate, $CH_3COOC_2H_5$, Sigma-Aldrich, St. Louis, MO) were employed. The molar composition was 1.5 Na_2SiO_3:1CTABr:361H_2O:7.4$CH_3COOC_2H_5$. Upon mixing all the reactants in homogeneous solution, the resulting sol was kept in a closed polypropylene flask at room temperature for 5 h, achieving a whitish color dispersion indicating silicon condensation. The synthesis of the solid particles then proceeded at 90 ºC for 50 h in the same open flask allowing for evaporation, without stirring. The product obtained was washed several times in distilled water and ethanol, and then filtered. To remove

the surfactant from the pores and activate the mesoporous structure, the MSSs were calcined at 600 ºC for 8 h with heating and cooling rates of 0.5 ºC/min.

Mixed matrix membrane (MMM) fabrication

For the membrane preparation, polysulfone (PSF) Udel® P-3500 (kindly supplied by General Electric Plastics Iberica, S.L., Barcelona, Spain) was degassed at 100 ºC for 4 h under vacuum to remove adsorbed water. This amorphous high performance polymer has excellent thermal and mechanical properties, and presents good solubility in many solvents such as dichloromethane, chloroform or tetrahydrofurane.

The first step was to fabricate the plain polymeric membrane for the purposes of comparison with those containing increased amounts of MSSs. For the pure membrane, 0.4 g of PSF was dissolved in 3.6 mL of chloroform and stirred for 1 day leading to a viscous solution. The fabrication procedure for the MMMs was identical to the pure polymer membrane preparation but with a previous dispersion stage of MSSs in the solvent (in a proportion of 90/10 wt.% solvent/MSS-polymer mixture, maintained constant for all cases) for 15 min in an ultrasonic bath. PSF was then added and the whole mixture was magnetically stirred for 1 day including three intervals of sonication for 15 min to assure a well-dispersed solution. The aggregation of MCM-41 between 0.6-0.9 µm particle sizes has been reported in the initial membrane formation, solved by stirring and sonicating the corresponding suspension several times[6]. Subsequently, the membranes were cast on flat glass plates, and then left overnight partially closed to slow down the natural evaporation of solvent under ambient conditions. The solutions were dried for 1 day at room temperature. Once dried, the films were placed for the same period under 10 mbar pressure in a VO 200 vacuum oven (Memmert, Schwabach, Germany) at 100 ºC to remove the remaining solvent. Membranes with different amounts of inorganic charge (4, 8, 12, 16 and 32 wt.%) were prepared. Thicknesses around 75-100 µm were measured using a Digimatic Micrometer (Quickmike Series 293-IP-54 Absolute 0-30 mm with an accuracy of ± 0.001 mm, Mitutoyo Corp., Kawasaki, Japan). A 15.2 cm^2 membrane area was cut from the film for permeation tests.

Membrane characterization techniques

The SEM images were collected on a JEOL JSM 6400 scanning electron microscope (Jeol Corp. Ltd., Tokyo, Japan) operating at 20 kV. For this purpose, cross sections were prepared by freeze-fracturing after immersion in liquid N_2. The good contact between both the dispersed MSSs and the continuous polymeric phase was also verified by TEM. It was necessary to embed a portion of the membrane in an Epofix™ cold-setting embedding resin (Electron Microscopy Sciences, Hatfield, PA). Consequently, in volume proportion, 15 parts of embedding resin and 2 parts of hardener were mixed, while the curing time was 8 h at room temperature, so that the cross section pieces could be sliced into the desired sections thin enough to be transparent for the electron beam. The slices were cut at 30-60 nm thickness using a RMC MT-XL ultramicrotome (RMC Products, Tucson, AZ) with a Standard Ultraknife 45º, 3 mm diamond blade (Drukker Ultra-microtome knife, Elementsix™, Cuijk, The Netherlands) able to slice hard materials such as molecular sieves. The sliced sections were stained in aqueous solution, placed on carbon copper grids and subsequently observed at 200 kV in a JEOL-2000 FXII TEM (Jeol Corp. Ltd., Tokyo, Japan.)

Thermogravimetric analyses were performed using Mettler Toledo TGA/SDTA 851^e equipment (Columbus, OH). Samples (10 mg) placed in 70 μL alumina pans were heated in air flow up to 850°C at a heating rate of 10 ºC/min. Differential scanning calorimetry (DSC) measurements were carried out using a Mettler Toledo DSC822^e (Columbus, OH) instrument to estimate the glass transition temperature (T_g) of the MMMs with growing percentages of MSSs. Approximately 15 mg of dried membrane was transferred to 40 μL aluminum pans, which were hermetically sealed with aluminum covers. The samples were first scanned from room temperature to 100 ºC with a heating rate of 10 ºC/min and then to 250 ºC at 2 ºC/min. Two consecutive runs of this method were performed for each sample and the glass transition temperature (T_g) was taken from middle point of the slope transition in the DSC curve as an average value based on the second run for a minimum of three samples.

Mechanical strength measurements of the membranes with different MSS loading were carried out under ambient conditions using a Dynamic Mechanical Analyzer (DMA) (01dB-Metravib, Limonest

Cedex, France) at a frequency of 2 Hz. Thin film strips with approximate dimensions of 0.1x5x10 mm were clamped in the jaws. Then, pre-tension (static displacement of 75 μm) was applied for undulating tension operation (dynamic displacement of 25 μm). Young´s moduli were obtained from the stiffness and the geometry of the sample.

BET specific surface area, N_2 isotherm and BJH pore size distribution (using the adsorption branch) were obtained for MSSs and grounded MSS-PSF MMMs with a TriStar 3000 porosity analyzer (Micromeritics Instrument Corp., Norcross, GA). The outgassing was done at 350ºC for 8h (MSSs) and 110, 175, 200 and 250ºC for 10-24 h (MSS-PSF MMMs) with a heating rate of 10 ºC/min.

Attenuated total internal reflection Fourier transform infrared (ATR-FTIR) spectroscopy of the membranes was performed on a Bruker Vertex 70 FTIR (Billerica, MA) spectrometer equipped with a DTGS detector and a Golden Gate diamond ATR accessory. Spectra were recorded by averaging 40 scans in the 4000-600 cm^{-1} wavenumber range at a resolution of 4 cm^{-1}. Data evaluation and spectra simulation were performed with OPUS software from Bruker Optics.

The X-ray photoelectron analysis (XPS) was performed with an Axis Ultra DLD (Kratos Tech., Manchester, U.K.). The specimens were mounted on a sample rod placed in the pretreatment chamber of the spectrometer and then evacuated at room temperature. The spectra were excited by the monochromatized AlKα source (1486.6 eV) run at 15 kV and 10 mA. For the individual peak regions, pass energy of 20 eV was used. The survey spectrum was measured at 160 eV pass energy. The surfaces were cleaned before measuring by sputtering the sample with an Ar^+ ion beam operating at 5 keV incident energy and with 20 mA current. Analyses of the peaks were performed with Casa XPS software, using a weighted sum of Lorentzian and Gaussian component curves after Shirley background subtraction. The binding energies were referenced to the internal C 1s (284.9 eV) standard.

Permeability measurements

The permeation module consists of two stainless steel pieces with a cavity to locate the membrane and a macroporous disk support 316LSS with 20 μm nominal pore size (Mott Corp., Farmington, CT) gripped inside with Viton® o-rings. A detailed description of the gas permeation equipment is presented elsewhere[5]. A mass-flow controlled (MC-100SCCM-D, Alicat Scientific, Tucson, AZ) 25/25 cm^3(STP)/min H_2/CH_4 or CO_2/N_2 stream was fed to the retentate side of the membrane at 275 kPa while the permeate side of the membrane was swept with a 1 cm^3(STP)/min mass-flow controlled stream of Ar (MC-5SCCM-D, Alicat Scientific, Tucson, AZ) at atmospheric pressure. When the CO_2/N_2 mixture was tested, He was used as the sweep gas (5 cm^3(STP)/min). Gas concentrations in the outgoing streams were analyzed by an on-line gas micro-chromatograph Agilent 3000A (Santa Clara, CA) equipped with TCD. Note than CO_2 partial pressure here was far below those values (> 5 atm) producing film plasticization[4]. Permeability in Barrer (1 Barrer = $1\cdot10^{-10}$ cm^3(STP)·cm/(cm^2·s·cmHg)) results were obtained once the exit stream of the membrane was stabilized. The separation selectivity was calculated as the ratio of permeabilities. All the permeation measurements were performed at 35 ºC controlled by an UNE 200 oven (Memmert, Schwabach, Germany).

RESULTS AND DISCUSSION

The gas transport behavior through a high quality MMM can be influenced by the intrinsic properties of the inorganic and organic materials, the compatibility or contact between phases avoiding interfacial voids, and the filler dispersion within the polymer matrix according to its morphology[10]. Besides, to achieve gas separation improvements for frequently used gas pairs the added amount of particles in polymeric MMM is usually excessive (zeolite loadings in the 30-40 wt.% range have often been used for gas separation[29, 30]), increasing materials and processing costs. In the case of polysulfone MMM using as filler mesoporous molecular sieves of the M41S family with loadings in the 10-40 wt.% range, the permeability increased with the loading, the best selectivity values being found at 10-20 wt.% loadings[6-8]. An optimal formulation of inorganic filler-polymer is envisaged to achieve increasing selectivities and permeabilities with the lowest filler percentage.

Table 1. BET specific surface area and accessible mesoporosity of MSSs, bare PSF membrane and 16 wt.% MSS-PSF MMM. Areas for MMMs are related to MSS mass. The standard deviation given below for BET specific surface area is that provided by the sorption device.

Sample	**Degassing temperature (ºC)**	**S_{BET} (m^2/g)**	**Accessible mesoporosity (%)**
Calcined MSS	350	1023±9	100
Bare PSF (pieces of ~5x5 mm^2)	175	0.4±0.0	-
	200	0.1±0.0	-
16 wt.% MSS-PSF MMM (pieces of ~5x5 mm^2)	110	1.7±1.2	0.2
16 wt.% MSS-PSF MMM (particles of ~ 0.15x0.15 mm^2)	110	38.3±0.1	3.7
	175	50.4±0.3	4.9
	200	35.9±0.2	3.5
	250	2.2±0.1	0.2

MSS-PSF MMMs

The MSSs used here have sizes in the 2-4 μm range[27, 28]. Low-angle X-ray diffraction for MSSs prepared by the same experimental procedure revealed a peak at 2.15º 2·theta[31], which corresponds to MCM-41 mesoporous phase[27]. The BET surface area for MSSs is 1023 m^2/g (see Table 1), higher than that reported (689 m^2/g) for BMS-3, which corresponds to mesoporous silica spheres prepared in the same way[27] and close to values reported for highly ordered MCM-41[32]. Figure S1 from the Supporting Information file shows a type IV N_2 isotherm for MSSs. The BJH analysis (Figure S2 from the

Supporting Information file) revealed a bimodal pore structure in MSSs with pores of 2.7 and 9 nm attributed, respectively, to MCM-41 and non-MCM-41 mesopores.

To investigate the dispersion of the mesoporous silica spheres within the polymer, cross sectional micrographs of the MMMs having 0, 4, 8, 12, 16 and 32 wt.% of MSSs (a) to f) in Figure S3 from the Supporting Information file) were examined by SEM. The filler distribution is apparently homogeneous and its presence is progressively more evident with increased loadings. Also, up to loadings of 16 wt.% continuous mesoporous silica-polymer matrix can be imagined, whereas at 32 wt.% loading the discontinuity is evident. In general, the observed roughness is the consequence of both protruding mesoporous silica spheres and empty spherical cavities of similar size and shape.

The BET specific surface area of MMS-PSF was investigated by N_2 adsorption at 77 K. Widely used to characterize porous solids, this technique is seldom applied to polymers due to the traditional consideration of polymers as nonporous substances[33]. In fact, the bare PSF do not show relevant BET specific surface areas after moderate degassing at a temperature (175 ºC) below that of glass transition (T_g, 188 ºC for pure PSF, as will be discussed later). In contrast, the MSS-PSF composite exhibited an optimum BET specific surface area of 50.4 m^2/g after degassing again at 175 ºC. The corresponding isotherm is depicted in Figure S1 from the Supporting Information file. Note that areas here for MMMs are related to MSS mass. A degassing temperature lower than 175 ºC was not efficient enough to remove solvent remains or adsorbed water while most of the chain joining bonds remained intact in their glassy polymer state. Degassing temperatures higher than T_g made the polymer soft and capable of chain deformation producing additional cross-linking that may reduce the accessible mesoporosity. The accessible mesoporosity was obtained dividing the corresponding BET specific surface area by that of the MSS sample. The low accessibility obtained (4.9 %, see Table 1) is compatible with the penetration of the polymer chains into the mesopores, as mentioned in the Introduction.

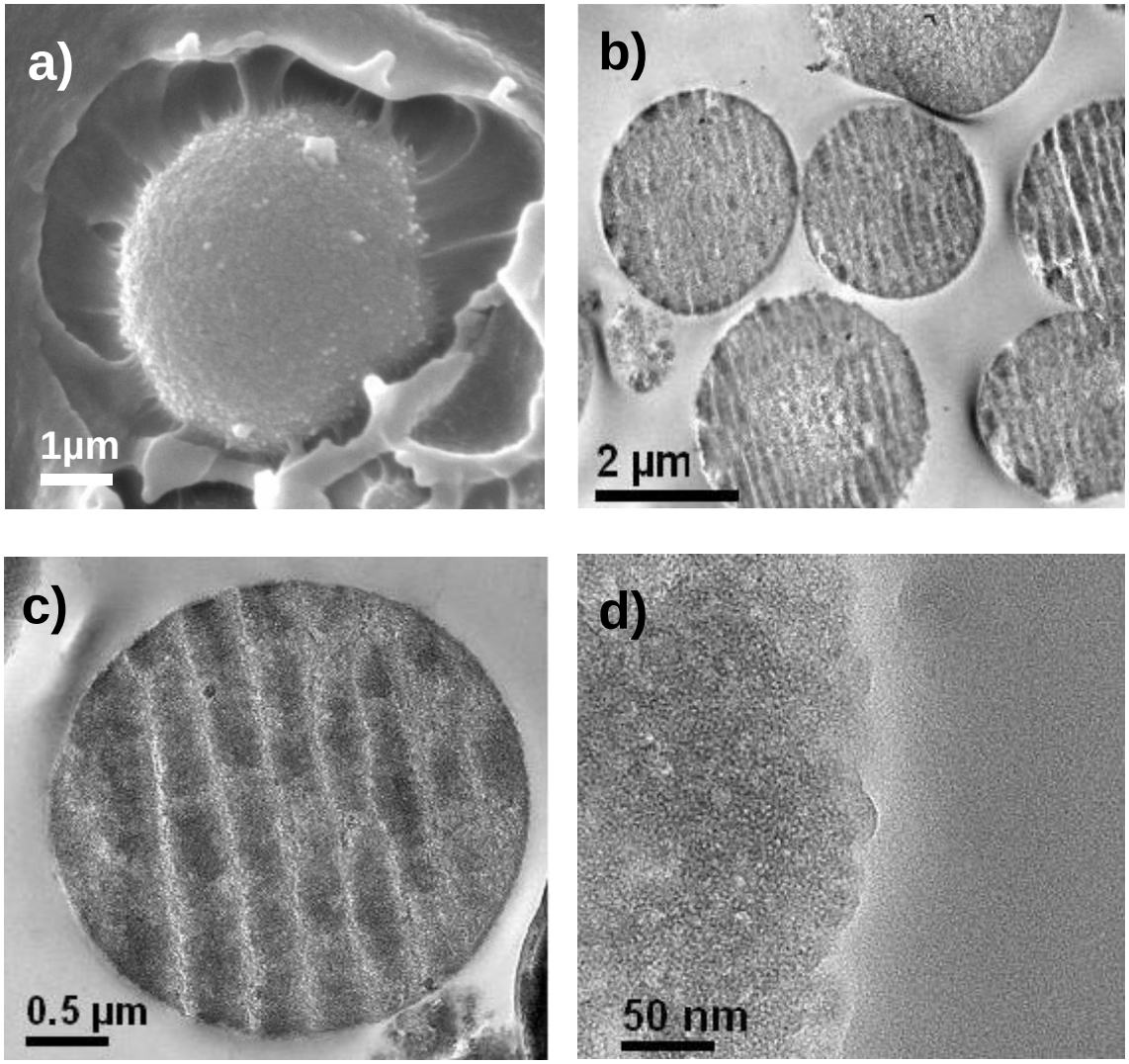

Figure 1. a) Cross section SEM image of a 8 wt.% MSS-PSF MMM; b) cross section TEM image of a 8 wt.% MSS-PSF MMM showing several MSSs; c) detail of one of the particles in b); d) detail of c), i.e. polymer-MSS interface. Note that the stripes in b) and c) were generated by the cutting with the diamond knife.

Furthermore, the penetration of the polymer chains into the mesoporosity of the filler gave rise to a real nanoporous composite even if the sphere size was in the micrometer range. This is illustrated by the SEM and TEM images in Figure 1, where a total absence of discontinuity is observed, even though the preparation of 30-60 nm slices (Figures 1b and 1c) with diamond ultramicrotome generated important shearing. In particular, the high magnification TEM image in Figure 1d reveals an intimate contact between both the inorganic and organic phases. Also, Figure S2 from the Supporting Information file, relating to the MSS-PSF MMM where the smaller mesopores and pore volume from

the BJH pore size distribution disappeared and decreased, respectively, is consistent with the penetration of polymer chains into the porosity of the filler. Moreover, Figure 1b allows one to discard agglomeration between particles, a phenomenon in which the sphericity of the particles, minimizing the contact between them, can play a decisive role. This figure shows a homogeneous group of well-defined, dispersed MSSs surrounded by polymer.

Thermal analysis and mechanical properties

TG curves in air of 0, 4, 8 and 16 wt.% of MSS-PSF MMMs are shown in Figure 2. In general, two apparent weight losses occurred at around 500-575 ºC and 600-750 ºC. The first weight loss, which could be attributed to pyrolysis processes in the atmosphere close to the sample releasing SO_2, benzene, phenol, toluene, styrene and xylene[34], ranges from 25 to 55 wt.%, depending on the MSS loading. The second accumulated weight loss is in the 83-100 wt.% range, and is a consequence of the complete degradation of the polymer chain allowing the verification of the nominal wt.% loading of inorganic filler present in the corresponding MMM, i.e. 0.7, 5.5, 10.6, and 16.8 wt.% residual contents, respectively. When MSSs with better thermal resistant properties and higher mechanical stiffness and strength (yielded by the Young's modulus) are incorporated into the polymer matrix, the resulting MMMs also offer improved mechanical properties although accompanied by increasing fragility. It can be noted that the thermal stability, at least in terms of weight loss, increased with the loading of MSSs, this being the expected behavior when inorganic-polymer nanocomposites are formed.[35-37] This is mainly due to the fact that the filler is a superior insulator and simultaneously improves mass transport barrier effects[38] to both the oxidizing atmosphere and the volatile compounds generated during degradation.

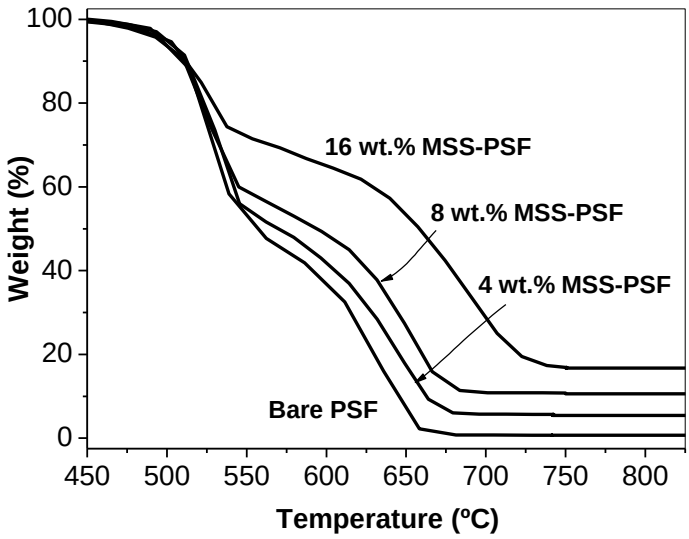

Figure 2. TGA weight losses versus temperature for 0, 4, 8, and 16 wt.% MSS-PSF MMMs.

Although the temperature of polymer decomposition is very high, the point that polymer chains change from the rigid to the rubbery state, known as the glass transition temperature (T_g), occurs earlier. When MMMs were prepared with calcined MSSs, there was a continuous increase in T_g as the MSS mass fraction increased, namely a 11 ºC difference: from 188.5 ºC at 0 wt.% to 199.5 ºC at 32 wt.% (see Figure 3). This is consistent with increasing rigidity and restricted motion of the polymer due to the chemical interactions established between chain polymer and MSS mesoporosity. An analogous T_g variation from 317 to 340 ºC for 0-30 wt.% mesoporous ZSM-5-polyimide MMMs has recently been reported[20]. However, when the MSS percentage was fixed at 8 wt.%, as expected, as-synthesized and chemically extracted MSSs gave rise to lower T_g values. TGA weight losses (not shown) were 42 and 8 wt.%, respectively, for as-made and extracted MSSs compared with the 5 wt.% loss obtained from the calcined MSSs.

Concerning mechanical properties, it can also be deduced from Figure 3 that the addition of MSSs within the polymer considerably increases Young´s modulus. This value substantially improves from 1.15 GPa for the pure PSF film to 1.85 GPa when the polymer is filled with 16% MSSs, the material becoming harder and stronger due to the stiffening effect of the rigid particles. These results are

consistent with those obtained when adding polystyrene/silylated MCM-48 nanocomposite particles to polystyrene[39] or incorporating polystyrene or poly(methylmethacrylate) filled mesoporous MCM-41 particles into polypropylene matrix[40].

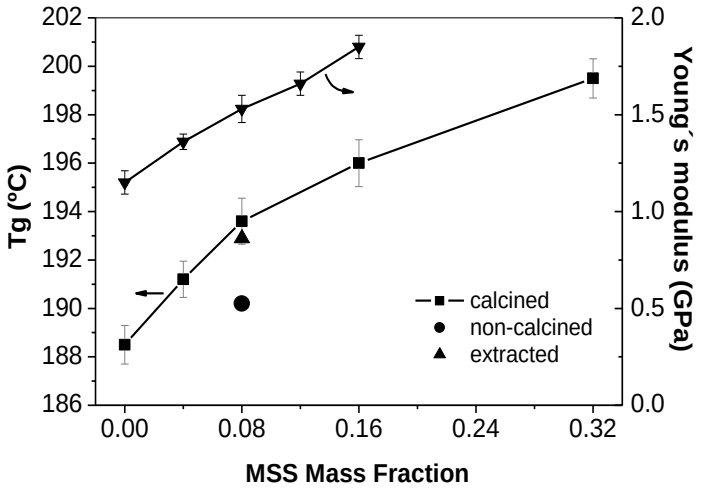

Figure 3. Glass transition temperature (T_g) and Young´s modulus as a function of MSS mass fraction for MSS-PSF MMMs. T_g of 8 wt.% calcined MSS-PSF is compared with as-synthesized (circle) MSS-PSF and extracted with solvent (triangle) MSS-PSF. In the extracted MSSs the surfactant was removed through Soxhlet treatment using an ethanol/HCl/water mixture including 250 mL of ethanol and 9 g of HCl (37 wt.%) per g of mesoporous silica at 55 ºC for 8 h.

ATR-FTIR and XPS characterization

Figure 4 shows FTIR spectra of MSSs, bare PSF and MSS-PSF MMMs with 8 and 32 wt.% MSS in the 1350-750 cm^{-1} wavenumber range. In the MSS spectrum there are broad absorption peaks at around 1230, 1070 and 800 cm^{-1} characteristic of asymmetric (Longitudinal Optical, LO, and Transversal Optical, TO, modes) and symmetric Si-O-Si stretching vibration, respectively[41]. The small shoulder band at 975 cm^{-1} is assignable to ν(Si-OH)[42]. The bare PSF membrane spectrum shows several peaks in this region: at 831, 852 and 872 cm^{-1} assigned to C-H rocking; at 1013, 1080 and 1103 cm^{-1} to C-C stretching; at 1147 and 1324 cm^{-1} to Ar-SO_2-Ar symmetric stretching; at 1168 cm^{-1} to C-C

stretching; at 1235 cm^{-1} to Ar-O-Ar stretching; and at 1294 cm^{-1} to S=O symmetric stretching[43]. Ar corresponds to aromatic. The 8 wt.% MSS-PSF MMM spectrum shows a shoulder at 1050 cm^{-1} that becomes an important feature in the 32 wt.% MSS-PSF MMM. This band is related to silica vibrations. Another interesting change can be observed in the peak associated to the aromatic-O-aromatic stretching vibration at about 1235 cm^{-1}. There is an increasing shift to higher wavenumbers with the SiO_2 concentration. The same effect was observed in polysulfone membranes with MCM-41 30 wt.% content[6]: the peak at 1232 cm^{-1} shifted to 1239 cm^{-1} upon introduction of the siliceous material. The high internal surface of mesoporous silica has OH groups which could interact via hydrogen-bonding with the aryl ether groups of the polymer. Similarly to non-spherical MCM-41 PSF membranes[6], no change in energy was observed for SO_2 stretching (1324, 1147 cm^{-1}) ruling out hydrogen-bonding through the sulfonyl oxygens.

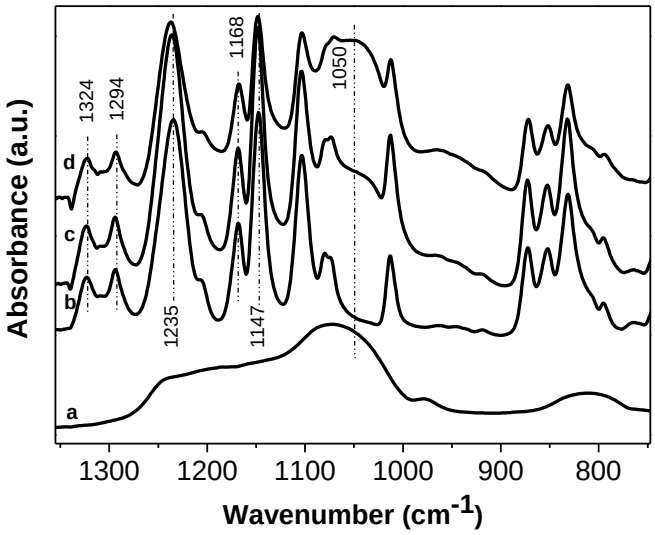

Figure 4. FTIR spectra of: a) MSSs, b) bare PSF, c) 8 wt.% MSS-PSF MMM, and d) 32 wt.% MSS-PSF MMM. PSF Udel® structural formula being 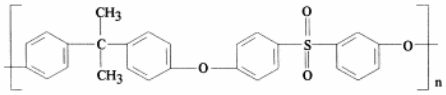 .

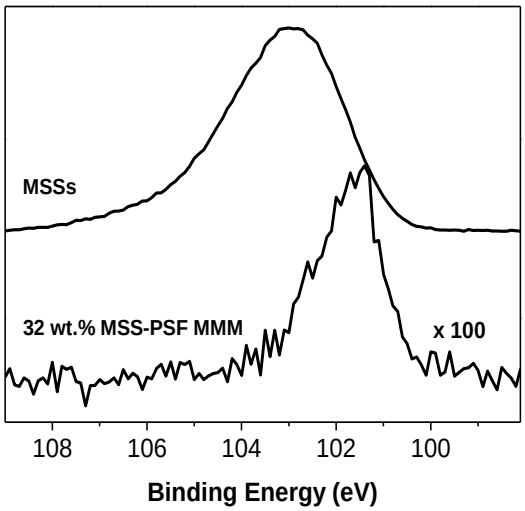

Figure 5. Si 2p core level for MSSs and 32 wt.% MSS-PSF MMM.

To further study the interaction between the polymer and the silica, XPS analyses were performed on the MSSs alone and on the MMM with the highest content of silica filler. The principal constituent elements of the PSF membrane after cleaning the surface were C, O, and S. Small concentrations of uncharacteristic PSF elements also found before cleaning were considered as impurities due to residual products from the membrane manufacture or environmental contamination[44]. On the other hand, the MSS spectrum only shows peaks related to O and Si besides the carbon from atmospheric contamination. The hybrid membrane spectra show peaks of C, O, S, Si and traces of Na; this last element was not detected after 10 min etching. Figure 5 shows the Si 2p spectra obtained on the 32 wt.% MSS-PSF MMM after cleaning the surface by etching. This membrane material was selected because the silica concentration gave a spectrum good enough for comparison. The binding energy (B.E.) measured for MSSs is 103.0 eV, e.g. typical for silicon atoms in mesoporous silica materials[45]. When incorporated into the polymeric film, the Si 2p B.E. shifted to lower values (101.9 eV) indicating a different electronic environment for the Si related to the aforementioned interaction between the silica particles and the polymer. This result is in agreement with that observed for chemically grafted mesoporous silica in the deconvolution of Si 2p spectra[46]. In this case, the-high-binding energy component (103.5 eV) was assigned to Si coordinated with oxide anions in SiO_2, whereas the lower-

binding-energy component (102.1 eV) was related to Si coordinated by oxide anions and an organic group.

Membrane separation performance

Since the addition of microporous fillers such as zeolites usually decreases the gas permeability of MMM[5], the mesoporous phase used here with bimodal pore distribution (2.7 and 9 nm) may favor gas diffusivity. Furthermore, it has been reported that ordered mesoporous silica (MCM-48) has a N_2 solubility coefficient more than 10 times higher than pure PSF[7]. With these two premises, it is not surprising that both H_2 and CH_4 permeabilities continuously increased with the MSS mass fraction in MSS-PSF MMMs (Table 2) from 11.8 and 0.20 Barrer, for pure PSF membrane (M1), to 108 and 3.2 Barrer, for 32 wt.% MSS-PSF MMM (M6). This increase in permeability also means that the penetration of the polymer chains would not affect the interior of the spheres, even though the pore openings of the MSSs were reduced until the disappearance to N_2 adsorption of the 2.7 nm pores (see Figure S2 from the Supporting Information file). Also, the increase in permeability has been attributed to the disruption of polymer chain packing and linking due to the presence of silica filler[47], leading probably to an increase in polymer free volume. Unlike permeabilities, H_2/CH_4 selectivity has an optimum of 79.2 (that of the bare polymer being 58.9) at 8 wt.% MSS content (sample M3). Loadings lower than 8 wt.% MSS did not alter significantly the MMM transport properties benefiting from the increase in rigidity of the polymer matrix (in agreement with the previous observations of T_g and Young´s modulus) and the Knudsen selectivity expected through the silica mesoporosity, which favor H_2 over CH_4 diffusion. An increase in both permeability and selectivity has also been reported in thin MMMs with non-porous silica particles as filler[47]. However, at higher MSS loadings, by-passing channels might connect surrounded voids existing between silica particles, as the 32 wt.% MSS-PSF MMM SEM image 2f suggests. In fact, at filler contents higher than or equal to 16 wt.%, the H_2/CH_4 selectivity is below that of the bare PSF membrane. The results given here for the bare PSF membrane are in good agreement with those in the literature: H_2 permeability = 11.8 Barrer and H_2/CH_4 selectivity = 53.6 at 35 ºC and 440 kPa of total pressure gradient[10].

Table 2. H_2/CH_4 separation performance at 35 ºC for the membranes prepared in this work. From samples M1 to M6 average values correspond for at least three different membranes.

Sample	MSS wt.%	Permeability (Barrer)		H_2/CH_4 Selectivity
		H_2	CH_4	
M1	0	11.8 (± 0.2)	0.20 (± 0.01)	58.9 (± 0.1)
M2	4	20.8 (± 0.7)	0.31 (± 0.01)	67.4 (± 2.1)
M3	8	26.5 (± 0.8)	0.34 (± 0.01)	79.2 (± 1.4)
M4	12	30.0 (± 2.9)	0.48 (± 0.02)	62.4 (± 3.7)
M5	16	47.9 (± 1.9)	0.87 (± 0.06)	55.7 (± 3.3)
M6	32	108 (± 4.1)	3.2 (± 1.10)	33.6 (± 6.4)
M7	8 (uncalcined)	42.5	0.78	54.3

The bare PSF membrane and the optimum loading 8 wt.% MSS-PSF membrane were tested for the CO_2/N_2 separation. Both CO_2 and N_2 permeabilities increased from 5.89 and 0.24 Barrer for pure PSF membrane to 12.6 and 0.35 Barrer for 8 wt.% MSS-PSF MMM. Similarly to H_2, which diffuses faster than CH_4 because of its smaller kinetic diameter (0.29 vs. 0.38 nm), CO_2 (0.33 nm) also diffuses faster than N_2 (0.36 nm). Moreover, the solubility coefficient in PSF is higher for CO_2 than for N_2 (2.1-4.0 vs. 0.15 $cm^3(STP)/(cm^3 \cdot atm)$)[10, 48], whereas the CO_2 adsorption capacity is much higher than that of N_2 for a similar size MCM-41 sample (namely, 16.3 vs. 1.9 $cm^3(STP)/g$ at 20 ºC)[49]. In consequence, the addition of optimum loading of mesoporous silica spheres gave rise to a clear improvement in terms of both CO_2 permeability and CO_2/N_2 selectivity, as shown in Figure 6 together with experimental CO_2/N_2 results achieved by other authors with 10 wt.% MCM-41[6, 8] or MCM-48[7] fillers. Note that the

improvement achieved in the present study is superior to others. Figure 6 also shows the results related to the H_2/CH_4 mixture.

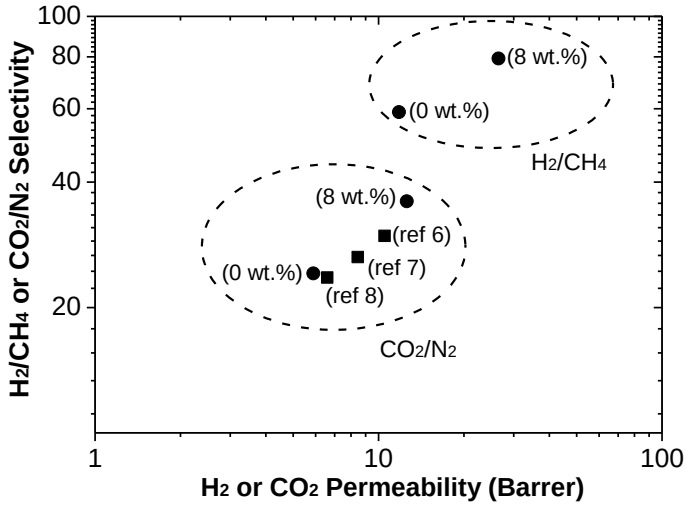

Figure 6. H_2/CH_4 or CO_2/N_2 selectivity as a function of H_2 or CO_2 permeability for 0 and 8 wt.% MSS-PSF MMMs (solid circles). For comparison, experimental CO_2/N_2 results achieved by other authors using 10 wt.% MCM-41[6, 8] or MCM-48[7] fillers are shown (solid squares).

Finally, the use of as made, uncalcined MSSs (sample M7 in Table 2) produced an important increase in the H_2 permeability linked to a decrease in selectivity. Figures 7a and in particular 7b suggest a lack of contact between phases when compared to Figure S3c from the Supporting Information file and Figure 1a, respectively. The template blocks the MSS pores and the polymer does not penetrate into the silica structure, creating holes between the polymer and MSS particles. This result suggests, as observed before[50], that not only enthalpic (hydrogen bonding with the OH-rich surface of the mesoporous spheres) factors are important when evaluating the interacting forces in a MMM but that entropic effects must be considered too. These entropic effects may be associated with the penetration of the polymer coils into the internal surface of the calcined mesoporous spheres evidenced from the aforementioned BET analysis.

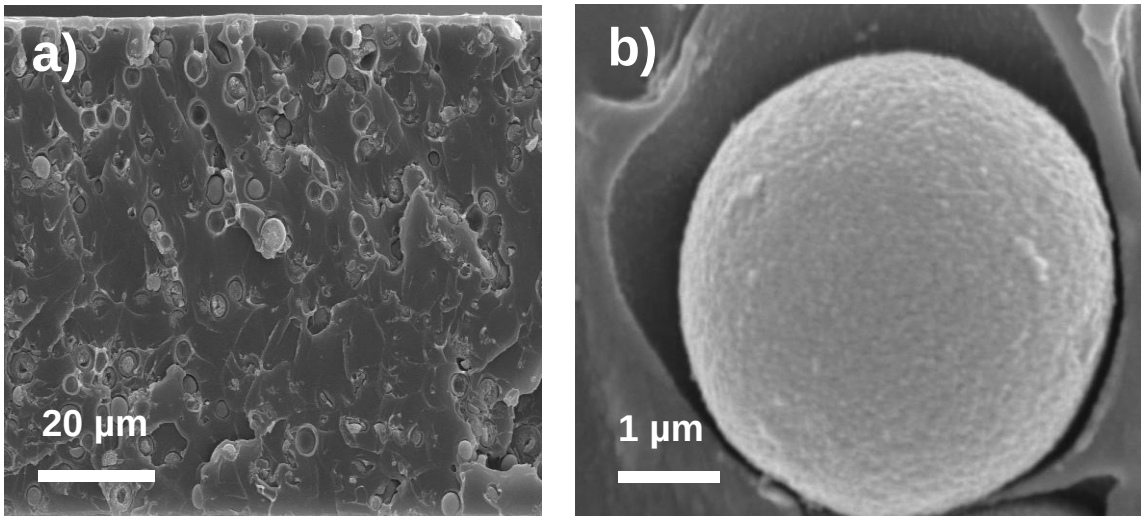

Figure 7. a) Cross section SEM image of 8 wt.% as-synthesized, uncalcined MSS-PSF MMM; b) detail of a).

CONCLUSIONS

Mixed matrix membranes of well-dispersed ordered mesoporous silica spheres and polysulfone can be prepared and efficiently used in the separation of H_2/CH_4 and CO_2/N_2 mixtures. Even though some properties or features continuously increased (the glass transition temperature and Young´s modulus) or monotonically evolved (SEM and TEM appearance, TGA ATR-FTIR and XPS analyses) with filler loading, an optimum H_2 permeability-H_2/CH_4 selectivity binomial was obtained at 8 wt.%. Loadings below 8 wt.% did not alter significantly the MMM transport properties and benefited from the increase in rigidity of the polymer matrix and the Knudsen selectivity expected through the silica mesoporosity, which favors H_2 over CH_4 diffusion. In contrast, loading over 8 wt.% created non-selective by-passing channels connecting surrounded voids existing between silica particles. Furthermore, the improvement in terms of permselectivity with the optimum loading was also reproduced with the CO_2/N_2 mixture.

From the ATR-FTIR spectra, it was possible to observe some interaction via hydrogen-bonding between the aryl ether groups of the polymer and the OH groups decorating the high internal surface of the mesoporous silica spheres. In agreement with this, XPS indicated a different electronic environment

for the Si atoms present in the mixed matrix membranes. These results together with the fact that the pore size and the wall thickness of the filler and the diameter of the polymer chain are within the order of 1 nanometer in size led us to consider the formation of a real composite membrane. In such a membrane, the polymer chains would penetrate into the mesoporosity of the silica spheres (as also suggested by the TEM and BET analyses). Finally, the good dispersion of the silica particles without appreciable agglomeration was attributed to both their spherical shape and size in the range of 2-4 μm.

ACKNOWLEDGEMENT

Financing from the Spanish Ministry of Education and Science (MAT2007-61028) is gratefully acknowledged. B. Zornoza also acknowledges a fellowship from the Spanish Science and Education Ministry (FPU Program).

SUPPORTING INFORMATION AVAILABLE

Figures S1 and S2 show N_2 isotherms and BJH pore size distributions for MSSs and 16 wt.% MSS-PSF MMM, whereas Figure S3 presents cross section SEM images of the MMMs having 0, 4, 8, 12, 16 and 32 wt.% MSSs. This information is available free of charge via the Internet at http://pubs.acs.org/.

REFERENCES

(1) Mahajan, R.; Koros, W. J. *Ind. Eng. Chem. Res.* **2000**, *39*, 2692-2696.

(2) Fawas, E. P.; Kapantaidakis, G. C.; Nolan, J. W.; Mitropoulos, A. C.; Kanellopoulos, N. K. *J. Mater. Process. Technol.* **2007**, *186*, 102-110.

(3) Baker, R. W. J. *Ind. Eng. Chem. Res.* **2002**, *41*, 1393-1411.

(4) Robeson, L. M. *J. Membr. Sci.* **2008**, *320*, 390-400.

(5) Gorgojo, P.; Uriel, S.; Téllez, C.; Coronas, J. *Microporous Mesoporous Mater.* **2008**, *115*, 85-92.

(6) Reid, B. D.; Ruiz-Trevino, A.; Musselman, I. H.; Balkus, K. J.; Ferraris, J. P. *Chem. Mater.* **2001**, *13*, 2366-2373.

(7) Kim, S.; Marand, E.; Ida, J.; Guliants, V. V. *Chem. Mater.* **2006**, *18*, 1149-1155.

(8) Kim, S.; Marand, E. *Microporous Mesoporous Mater.* **2008**, *114*, 129-136.

(9) Merkel, T. C.; Freeman, B. D.; Spontak, R. J.; He, Z.; Pinnau, I.; Meakin, P.; Hill, A. J. *Science* **2002**, *296*, 519-522.

(10) Ahn, J.; Chung, W.-J.; Pinnau, I.; Guiver, M. D. *J. Membr. Sci.* **2008**, *314*, 123-133.

(11) Vu, D. Q.; Koros, W. J.; Miller, S. J. *J. Membr. Sci.* **2003**, *211*, 335-348.

(12) Cong, H. L.; Zhang, J. M.; Radosz, M.; Shen, Y. Q. *J. Membr. Sci.* **2007**, *294*, 178-185.

(13) Kim, S.; Chen, L.; Johnson, J. K.; Marand, E. *J. Membr. Sci.* **2007**, *294*, 147-158.

(14) Zimmerman, C. M.; Singh, A.; Koros, W. J. *J. Membr. Sci.* **1997**, *137*, 145-154.

(15) Chung, T. S.; Jiang, L. Y.; Li, Y.; Kulprathipanja, S. *Prog. Polym. Sci.* **2007**, *32*, 483-507.

(16) Gur, T. M. *J. Membr. Sci.* **1994**, *93*, 283-289.

(17) Jiang, L. Y.; Chung, T. S.; Kulprathipanja, S. *AIChE J.* **2006**, *52*, 2898-2908.

(18) Li, Y.; Guan, H. M.; Chung, T. S.; Kulprathipanja, S. *J. Membr. Sci.* **2006**, *275*, 17-28.

(19) Chen, Z. W.; Holmberg, B.; Li, W. Z.; Wang, X.; Deng, W. Q.; Munoz, R.; Yan, Y. S. *Chem. Mater.* **2006**, *18*, 5669-5675.

(20) Zhang, Y.; Balkus Jr, K. J.; Musselman, I. H.; Ferraris, J. P. *J. Membr. Sci.* **2008**, *325*, 28-39.

(21) Boyer, R. F.; Miller, R. L. *Macromolecules* **1977**, *10*, 1167-1169.

(22) Ruben, G. C.; Stockmayer, W. H. *Proc. Natl. Acad. Sci. U.S.A.* **1992**, *89*, 7991-7995.

(23) Ravikovitch, P. I.; Neimark, A. V. *Langmuir* **2000**, *16*, 2419-2423.

(24) Schumacher, K.; Ravikovitch, P. I.; Du Chesne, A.; Neimark, A. V.; Unger, K. K. *Langmuir* **2000**, *16*, 4648-4654.

(25) Gierszal, K. P.; Jaroniec, M.; Kim, T. W.; Kim, J.; Ryoo, R. *New J. Chem.* **2008**, *32*, 981-993.

(26) Kumar, D.; Schumacher, K.; von Hohenesche, C. D. F.; Grun, M.; Unger, K. K. *Colloids Surf. A* **2000**, *187*, 109-116.

(27) Schulz-Ekloff, G.; Rathousky, J.; Zukal, A. *J. Inorg. Mater.* **1999**, *1*, 97-102.

(28) Navascues, N.; Tellez, C.; Coronas, J. *Microporous Mesoporous Mater.* **2008**, *112*, 561-572.

(29) Tantekin-Ersolmaz, S. B.; Atalay-Oral, Ç.; TatlIer, M.; Erdem-Senatalar, A.; Schoeman, B.; Sterte, J. *J. Membr. Sci.* **2000**, *175*, 285-288.

(30) Golemme, G.; Bruno, A.; Manes, R.; Muoio, D. *Desalination* **2006**, *200*, 440-442.

(31) Casado, C.; Bosque, J.; Navascués, N.; Téllez, C.; Coronas, J. *Microporous Mesoporous Mater.* **2009**, *120*, 69-75.

(32) Kruk, M.; Jaroniec, M.; Kim, J. H.; Ryoo, R. *Langmuir* **1999**, *15*, 5279-5284.

(33) Ilinitch, O. M.; Fenelonov, V. B.; Lapkin, A. A.; Okkel, L. G.; Terskikh, V. V.; Zamaraev, K. I. *Microporous Mesoporous Mater.* **1999**, *31*, 97-110.

(34) Molnár, G.; Botvay, A.; Pöppl, L.; Torkos, K.; Borossay, J.; Máthé, Á.; Török, T. *Polym. Degrad. Stab.* **2005**, *89*, 410-417.

(35) Sinha Ray, S.; Okamoto, M. *Prog. Polym. Sci.* **2003**, *28*, 1539-1641.

(36) Kim, H.-S.; Chen, G.-X.; Jin, H.-J.; Yoon, J.-S. *Colloids Surf. A* **2008**, *313-314*, 56-59.

(37) Sur, G. S.; Sun, H. L.; Lyu, S. G.; Mark, J. E. *Polymer* **2001**, *42*, 9783-9789.

(38) Solovyov, S. E. *J. Phys. Chem. B* **2006**, *110*, 17977-17986.

(39) He, J.; Shen, Y.; Evans, D. G. *Microporous Mesoporous Mater.* **2008**, *109*, 73-83.

(40) Wang, N.; Shao, Y.; Shi, Z.; Zhang, J.; Li, H. *Mater. Sci. Eng. A* **2008**, *497*, 363-368.

(41) Muroya, M. *Colloids Surf. A* **1999**, *157*, 147-155.

(42) Khalil, K. M. S.; Makhlouf, S. A. *Appl. Surf. Sci.* **2008**, *254*, 3767-3773.

(43) Pihlajamaki, A.; Vaisanen, P.; Nystrom, M. *Colloids Surf. A* **1998**, *138*, 323–333.

(44) de Lara, R.; Benavente, J. *J. Colloid Interface Sci.* **2007**, *310*, 519-528.

(45) Kim, K.; Lee, H. B.; Shin, K. S. *Langmuir* **2008**, *24*, 5893-5898.

(46) Capel-Sanchez, M. C.; Barrio, L.; Campos-Martin, J. M.; Fierro, J. L. G. *J. Colloid Interface Sci.* **2004**, *277*, 146-153.

(47) Moaddeb, M.; Koros, W. J. *J. Membr. Sci.* **1997**, *125*, 143-163.

(48) Aitken, C. L.; Koros, W. J.; Paul, D. R. *Macromolecules* **1992**, *25*, 3424-3434.

(49) Macario, A.; Katovic, A.; Giordano, G.; Iucolano F.; Caputo, D. *Microporous Mesoporous Mater.* **2005**, *81*, 139-147.

(50) Shu, S.; Husain, S.; Koros, W. J. *J. Phys. Chem. C* **2007**, *111*, 652-657.

TOC graphic
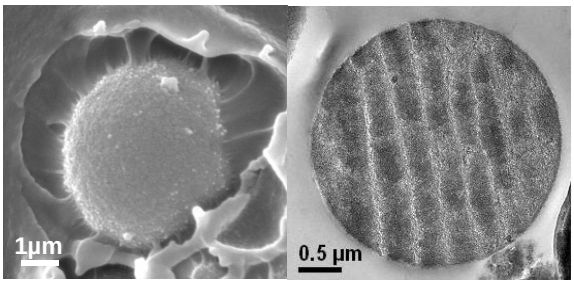
Beatriz Zornoza, Silvia Irusta, Carlos Téllez and Joaquín Coronas* *Langmuir,* **2009** *Mesoporous silica sphere-polysulfone mixed matrix membranes with optimum filler loading for gas separation*